AQUA
Water Infrastructure, Ecosystems and Society

IWA PUBLISHING

 AQUA — Water Infrastructure, Ecosystems and Society Vol 73 No 1, 114 doi: 10.2166/aqua.2024.289

Effects of porous structures on point source dispersion across the sediment–water interface

Pengcheng Xu[a,b,c], Lingling Wang[a,b,c], Jin Xu[a,b,c], Zhe Wang[a], Soeren Ahmerkamp[d], Gerhard Bartzke[e], Mengtian Wu[a], Jianjun Han[a,b,c] and Hai Zhu[a,b,c,*]

[a] State Key Laboratory of Hydrology-Water Resources and Hydraulic Engineering, Hohai University, Nanjing 210098, China
[b] College of Water Conservancy and Hydropower Engineering, Hohai University, Nanjing 210098, China
[c] Key Laboratory of Hydrologic-Cycle and Hydrodynamic-System of Ministry of Water Resources, Hohai University, Nanjing 210098, China
[d] Department of Biogeochemistry, Max Planck Institute for Marine Microbiology, Bremen 28359, Germany
[e] MARUM-Center for Marine Environmental Sciences, Universität Bremen, Bremen 28359, Germany
*Corresponding author. E-mail: h.zhu@hhu.edu.cn

ABSTRACT

Understanding the transport of point source solutes across the sediment–water interface (SWI) is important for the protection of river environments. Conventional coupled models assume the porous media layer as Darcy's laminar flow and therefore cannot accurately capture the transport processes within the porous media. Furthermore, the effect of the porous structure of the riverbed on the transport process is largely unknown. In this study, we performed pore-scale numerical simulations of point source solutes transport across the SWI to investigate the effects of different porous structures in the riverbed on flow and point source dispersion. By solving the Reynolds-averaged Navier–Stokes equations with the k–ω shear stress transport turbulence closure model, we determine the complex flow field information and the spatial distribution of point source solutes for the coupled model. The results indicate that the presence of porous structures creates recirculation zones in the coupled model, which prevents turbulent structures reaching deeper layers. Random porous structures induce more preferential flow, inhibit the formation of recirculation zones, and exhibit higher solute dispersion, which is directly related to turbulent solute fluxes. Furthermore, our study reveals that the release position of point sources significantly influences the distribution of solute concentrations within the porous bed.

Key words: point source, porous structures, preferential flow, recirculation zones, sediment–water interface

HIGHLIGHTS

- The influence of porous structures on flow and point source dispersion is elucidated within a coupled system of overlying water and porous media.
- Random porous structures will induce more preferential flow and accelerate solute transport.
- The presence of preferential flow inhibits the formation of recirculation zones.
- Turbulent solute flux explains the wider distribution of random porous structures.

1. INTRODUCTION

The sediment–water interface (SWI) is one of the most important interfaces in aquatic ecosystems, controlling the solute exchange process between the overlying water layer and the porous media layer, which can greatly influence the health and function of aquatic ecosystems (Grant *et al.* 2012; Han *et al.* 2018; Hester *et al.* 2019; Shen *et al.* 2020; Wu *et al.* 2023). The turbulence of the overlying water causes an uneven pressure distribution at the SWI, and the pressure drives the overlying water into the porous media layer. Nutrients and toxicants from the overlying water are transported across the SWI to the porous media layer, where a series of biogeochemical reactions occur and then the mineralised and remineralised products are released by the sediments to return to the overlying water, resulting in secondary pollution of the water body (Janssen *et al.* 2012; Boano *et al.* 2014; Lian *et al.* 2019). These processes are determined by the solute exchange processes in the vicinity of the SWI, as described in Figure 1 (Scalo *et al.* 2012; Ahmerkamp *et al.* 2015; Kim *et al.* 2020). Hence,

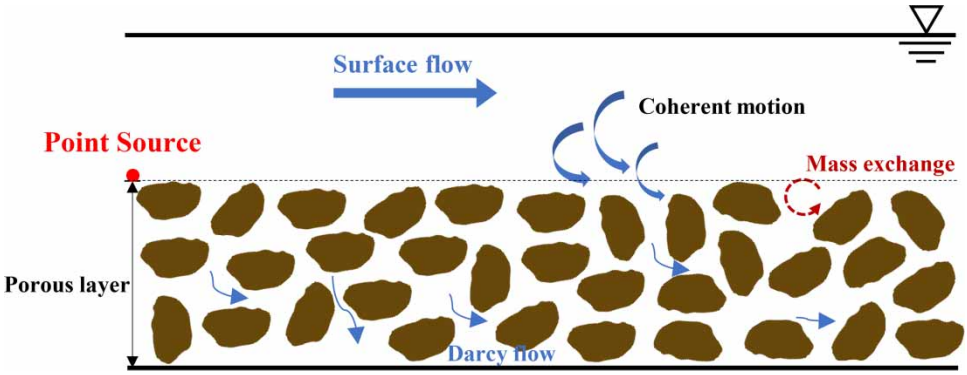

Figure 1 | Schematic of surface–subsurface water interaction near the SWI.

accurate simulation and analysis of flow and solute transport characteristics in the vicinity of SWI is essential for understanding the functioning of aquatic ecosystems (Hester *et al.* 2013; Blois *et al.* 2014; Fang *et al.* 2018; He *et al.* 2019).

For the coupling model of overlying water and porous media, the conventional models usually represent the porous media layer as Darcy's laminar flow, which has been proven to simulate solute transport in fine-grained riverbeds (Cardenas & Wilson 2007a; Janssen *et al.* 2012; Hester *et al.* 2019). However, this approach has limitations in modelling solute exchange processes in coarse-grained riverbeds and usually underestimates the exchange flux across the SWI. This is mainly because the extended turbulence into the transition layer, commonly ignored in conventional models, significantly contributes to solute exchange processes near the SWI and accelerating solute transport from the overlying water into the porous medium (Reidenbach *et al.* 2010; Han *et al.* 2018; Lian *et al.* 2019; Roche *et al.* 2018). Moreover, this modelling approach also underestimates the inertial effects of complex pore scales in porous media layers, which includes preferential flow and recirculation zones for interfacial solute exchange (Bottero *et al.* 2013; Zhou *et al.* 2019; Kim *et al.* 2023). The interfacial mass flux induced by overlying water turbulence is six times higher in coarse-grained riverbeds than in fine-grained riverbeds, as demonstrated by Reidenbach *et al.* (2010). Therefore, the assumption of a porous media layer as Darcy's laminar flow is not suitable in modelling coarse-grained riverbeds, and it may significantly underestimate the interfacial mass exchange flux.

Recent studies based on direct measurements indicate that the turbulence of the overlying water directly affects the flow characteristics within the porous media layer and that a recirculation zone is formed in the porous space near the SWI, which may serve as a temporary storage area for solutes that can be subsequently re-released into the overlying water (Blois *et al.*2012; Bolster *et al.* 2014; Roche *et al.* 2018). This anomalous solute transport characteristic deviates from Fick's law (Crevacore *et al.* 2016; Kim *et al.* 2020). Therefore, we need to clarify the solute transport properties within the porous structure to better understand the non-Fickian characteristics of the solute transport process.

Furthermore, several studies on coupled modelling of overlying water and porous media at the pore scale usually idealise the porous media layer as regularly arranged circular or square particles (Prinos *et al.* 2003; Fang *et al.* 2018; Lian *et al.* 2019; Kim *et al.* 2020; Cho *et al.* 2022; Singh *et al.* 2022). To the best of our knowledge, only a limited number of studies have explored the effects of irregular distributions. These investigations have revealed that the arrangement of porous structures not only influences the flow of pore water but also has a significant impact on the overall flow pattern of the coupled model (Bartzke *et al.* 2014; Suga *et al.* 2020; Shen *et al.* 2021; Kim *et al.* 2023). Random porous structures produce distinct stagnation zones and preferential flows, which directly affect the solute transport process across the SWI; therefore, a more comprehensive understanding of the effect of porous structures on flow transport patterns is necessary.

In nature, the sources of solute pollution in overlying water are mainly from the discharge of industrial wastewater and domestic sewage, and such inputs from specific pollution sources are collectively referred to as point sources (Pal *et al.* 2010; Li 2014). Point source pollution of rivers may include chemicals, organics, heavy metals, nutrients, and so on, which may have direct impacts on water ecosystems (Wilhelm 2009; Hou *et al.* 2021). However, although riverine point source pollution is a common mode of solute diffusion, the exact mechanism of its diffusion at the pore scale is unknown.

In this study, we developed a pore-scale coupled model of overlying water and porous media, and further evaluated the effects of regular and random porous structures on the flow characteristics and point source dispersion characteristics of the coupled model. To achieve this, we utilise a 2D k–ω shear stress transport (SST) turbulence model to accurately resolve

the flow characteristics of the coupled pore-scale model. Once the flow field is sufficiently developed, we release a point source consisting of non-reactive solutes at the SWI to analyse and obtain the spatial distribution characteristics of solute transport for the coupled model. Then, the effect of Reynolds numbers on the coupled model flow and dispersive transport of the point source is further explored. Furthermore, the turbulent solute flux is utilised to establish the relationship between interfacial turbulence and solute diffusion. In addition, we explore the variability of different release positions of the point source to gain further insights into the dispersion process.

2. METHODS

2.1. Hydrodynamic model

To accurately capture the segregated flow in the complex structure of porous media, we analyse the hydrodynamic properties of a coupled model of overlying water and porous media using the Reynolds-averaged Navier–Stokes equations with the k–ω SST turbulence closure model. The model combines the advantages of both the k–ε and the k–ω turbulence models to better handle adverse pressure gradients and flow separation, which is particularly effective in predicting the behaviour of boundary layers and turbulent flows with complex vortex structures near walls (Menter 1994; Menter *et al.* 2003; Lee *et al.* 2021; Sarmiento-Laurel *et al.* 2022).

We conducted numerical simulations using an unsteady RANS solver integrated with the k–ω SST turbulence model, which is available in the OpenFOAM library. The continuity and momentum equations are as follows:

$$\frac{\partial U_i}{\partial x_i} = 0 \tag{1}$$

$$\frac{\partial U_i}{\partial t} + U_j \frac{\partial U_i}{\partial x_j} = -\frac{1}{\rho}\frac{\partial P}{\partial x_i} + \frac{\partial}{\partial x_j}\left[v\left(\frac{\partial U_i}{\partial x_j} + \frac{\partial U_j}{\partial x_i}\right)\right] - \frac{\partial}{\partial x_j}\overline{u_i u_j} \tag{2}$$

where U_i and U_j are the time-averaged velocity components in the x_i and x_j directions, respectively; t is the time; P is the fluid pressure; ρ is the density of the fluid; ν is the kinematic viscosity of fluid; u_i and u_j are the fluctuating velocity vectors in the x_i and x_j directions, respectively; and $-\overline{u_i u_j}$ is the Reynolds stress, which is a product of the Reynolds decomposition defined as

$$-\overline{u_i u_j} = v_t\left(\frac{\partial U_i}{\partial x_j} + \frac{\partial U_j}{\partial x_i}\right) + \frac{2}{3}k\delta_{ij} \tag{3}$$

where v_t is the turbulent eddy viscosity, k is the turbulent kinetic energy, and δ_{ij} is the Kronecker delta. As previously mentioned, we employ the k–ω SST turbulence model to solve Equation (2). The turbulent kinetic energy k and the specific dissipation ω are computed by solving the following additional conservation equations:

$$\frac{\partial(k)}{\partial t} + \frac{\partial(U_j k)}{\partial x_j} = \rho\tau_{ij}\frac{\partial U_i}{\partial x_j} - \beta^*\rho\omega k + \frac{\partial}{\partial x_j}\left[(\mu + \mu_t\sigma_k)\frac{\partial k}{\partial x_j}\right] \tag{4}$$

$$\frac{\partial(\omega)}{\partial t} + \frac{\partial(U_j \omega)}{\partial x_j} = \alpha\frac{\rho\omega}{k}\tau_{ij}\frac{\partial U_i}{\partial x_j} - \beta\rho\omega^2 + \frac{\partial}{\partial x_j}\left[(\mu + \mu_t\sigma_\omega)\frac{\partial \omega}{\partial x_j}\right] \tag{5}$$

The closure coefficients α, β, β^*, σ_k, and σ_ω are 5/9, 3/40, 9/100, 1/2, and 1/2, respectively (Menter 1993).

2.2. Non-reactive solute transport model

In this study, the point source consists of non-reactive solutes, and only the effect of hydrodynamic processes on solute migration and diffusion is considered, without taking into account the reactive transport processes of solutes, which is the same as in previous studies (Tanino & Nepf 2008; Jin *et al.* 2010; Guo *et al.* 2022).

Therefore, point source solutes can be characterised by the generalised advection–diffusion equation (Jin *et al.* 2010; Rubol *et al.* 2016; Ai *et al.* 2022), calculated as follows:

$$\frac{\partial C}{\partial t} + U_j\frac{\partial C}{\partial x_j} = \frac{\partial}{\partial x_j}\left[(D + D_t)\frac{\partial C}{\partial x_j}\right] \tag{6}$$

where C is the solute concentration and D and D_t are the molecular and turbulent diffusion coefficients, which can be defined as follows:

$$D = \frac{\nu}{Sc} \tag{7}$$

$$D_t = \frac{\nu_t}{Sc_t} \tag{8}$$

where Sc and Sc_t are the molecular and turbulent Schmidt numbers, respectively.

2.3. Setup of numerical experiments

2.3.1. Model validation cases

To validate the accuracy of the hydrodynamic model, we used experimental data from Prinos *et al.* (2003). They conducted hydraulic experiments in a 10- m-long and 0.25-m-wide experimental flume with hydraulically smooth walls and an underlying permeable bed consisting of regular rods, which investigated the 2D hydrodynamic characteristics, as shown in Figure 2. The experiment parameters are listed in Table 1, which display the geometric and hydrodynamic characteristics of the flow. The overlying water depth (H_f) is 0.03 m, the porous layer depth (H_p) is 0.055 m, the rod diameter (d) is 0.01 m, and the porosity (ϕ) is 0.8286, respectively.

Based on these experiment parameters, Prinos *et al.* (2003) conducted numerical simulations using the 2D RANS equations based on the standard k–ε turbulence model. Furthermore, we compared the model results with the numerical simulation

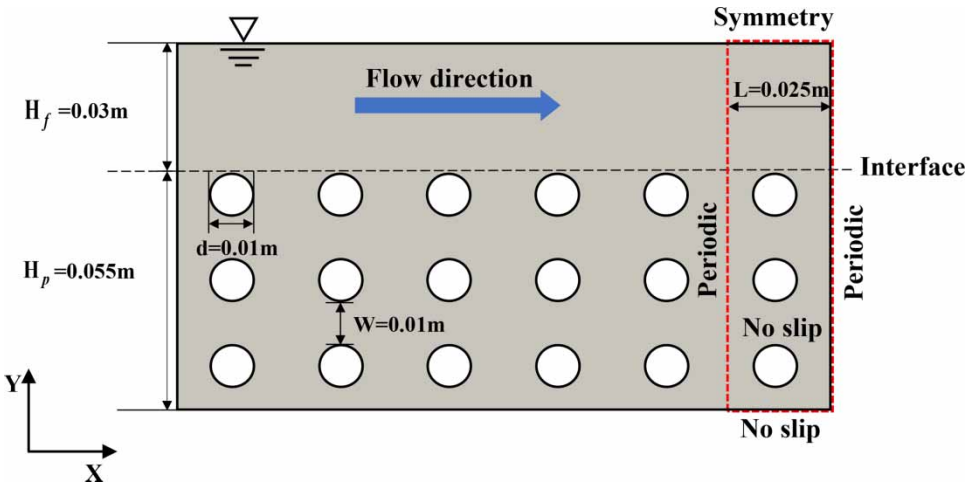

Figure 2 | Schematic diagram of the validation case from Prinos *et al.* (2003).

Table 1 | The validation case parameter setting from Prinos *et al.* (2003)

Parameter	Description	Value
H_f(m)	Overlying water depth	0.03
H_p(m)	Porous layer depth	0.055
ϕ	Porosity	0.8286
U_*(m/s)	Shear velocity	0.0243
Re_f	Reynolds number	7.581×10^3
K(m^2)	Permeability	4.107×10^{-4}

results of Kim *et al.* (2020) using the renormalization group (RNG) k–ε turbulence model to demonstrate the advantages of the k–ω SST turbulence model in dealing with flow in complex porous media.

Regarding the validation of the non-reactive solute transport model, we compared the simulation results with the results of the analytical solution of Aral & Liao (1996). The analytical solution equation is described as follows:

$$C(x, y_0, t) = \frac{C_0}{4\pi Dt}\exp\left(-\frac{(x - x_0 - ut)^2}{4Dt}\right) \tag{9}$$

where (x_0, y_0) is the position of point source, C_0 is the initial concentration, D is the diffusion coefficient, and u is the velocity in the flow field.

First, we created a 100×100 square computational domain with dx and dy of 1. The point source is released at position (50, 50). In this study, D and u were set to 0.001 and 0.01, respectively.

2.3.2. Study cases

After validating the accuracy of the hydrodynamic model and the non-reactive solute transport model, we coupled the two models to further investigate the flow and point source solute transport characteristics of the coupled model of overlying water and porous media composed of two different porous structures (regular and random) with a porosity of 0.636; the geometry and dimension are shown in Figure 3. In addition, we investigated the effect of different Reynolds numbers on hydrodynamics by varying the inlet velocity. Here, the pore diameters were set the same as those in the experiment setup by Prinos *et al.* (2003), which can be considered coarse-gravel beds. H_f and H_p are 0.0325 and 0.0575 m, respectively.

When the turbulence is sufficiently developed, we applied a point source at position $y/H = 0$, to assess the dispersion of the point source at the SWI. The simulation parameters are summarised in Table 2. In the case name, Regular002, Regular010, Random002, and Random010 represent two regular porous structure cases and two random porous structure cases, respectively. Note that 002 and 010 denote inlet velocities $U_{in} = 0.02$ and 0.10 m/s, respectively.

2.3.3. Boundary conditions

We apply the rigid lid assumption to the upper boundary when the Froude number $\mathrm{Fr} = U_f/\sqrt{gH_f} < 1$, which neglects the fluctuation of the free water surface. This approach is widely used in the application of open channel flows (Van Balen *et al.* 2010; Janssen *et al.* 2012; Chen *et al.* 2018). No-slip boundary conditions are applied to the bottom and the porous structure surfaces. Periodic boundary conditions are implemented in streamwise directions, as illustrated in Figure 2. It is worth noting that since solute migration does not apply to the periodic boundary conditions, to prevent re-entry of the solute from the inlet, we set the scalar value of the inlet close to the release position of the point source to zero and solute migration to a single cycle. The computations were performed on the Hohai High-Performance Computing Center.

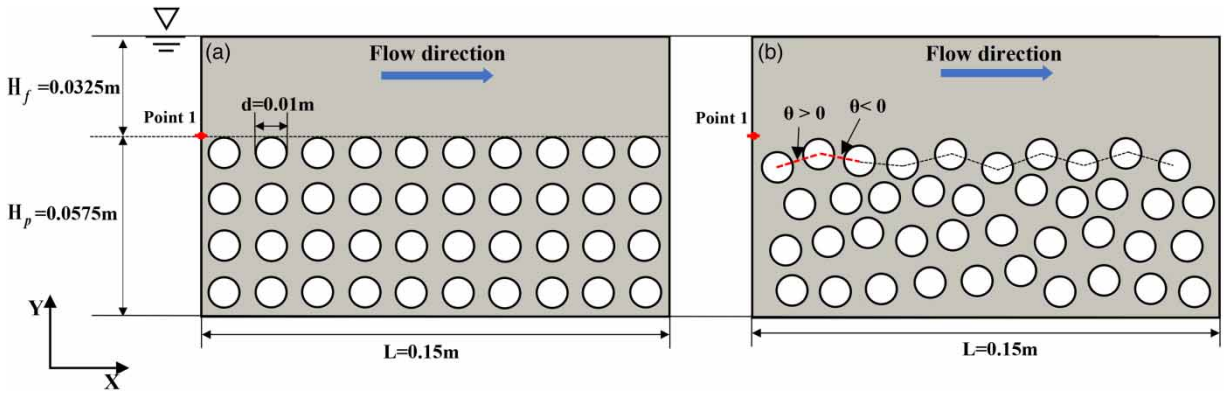

Figure 3 | Schematic diagram of the study cases with different porous structures. (a) represents the regular porous structures case and (b) represents the random porous structures case, which have the same porosity.

Table 2 | The parameter setting for the study cases

Parameter	Description	Regular002	Regular010	Random002	Random010
H_f(m)	Overlying water depth	0.0325	0.0325	0.0325	0.0325
H_p(m)	Porous layer depth	0.0675	0.0675	0.0675	0.0675
ϕ	Porosity	0.636	0.636	0.636	0.636
U_{in}(m/s)	Inlet velocity	0.02	0.10	0.02	0.10
U_f(m/s)	Mean surface velocity	0.0427	0.2588	0.0291	0.2033
U_*(m/s)	Shear velocity	0.0033	0.0171	0.0029	0.0145
Fr	Froude number	0.07	0.46	0.05	0.36
Re_f	Reynolds number	1,388	8,411	946	6,607

3. RESULTS AND DISCUSSION

3.1. Results of model validation

Figure 4 shows that the vertical mean velocity profile and turbulent kinetic energy profile for the validation case, normalised by the shear velocity, is approximated as $U* = \sqrt{\tau_{\max}/\rho}$ and suggested by Voermans *et al.* (2017). We compare the simulation results with the experimental results of Prinos *et al.* (2003) and obtain a good agreement, which also illustrate the accuracy of our model. As shown in Figure 4(a) and 4(b), the mean velocity in the overlying water of the coupled model reduces significantly at the SWI due to the presence of the porous structures, which hinders further development of the overlying water, and significant momentum exchange occurs, resulting in the generation of slip velocity at the SWI. Furthermore, compared with the conventional k–ε and RNG k–ε turbulence models, the k–ω SST turbulence model used in this paper has significant advantages in effectively solving complex flow structures due to the fact that it provides an improved representation of the

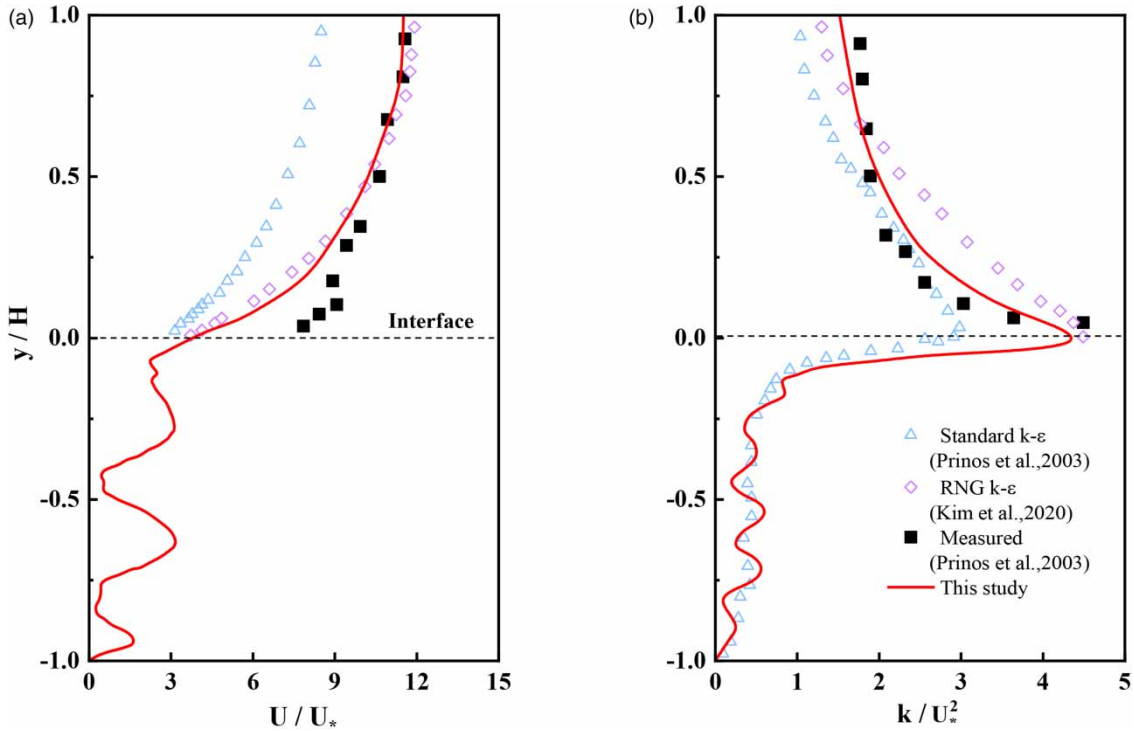

Figure 4 | Comparison of our model results with experimental and numerical data from Prinos *et al.* (2003) and Kim *et al.* (2020). (a) and (b) are the vertical mean flow velocity profiles and turbulent kinetic energy profiles, respectively.

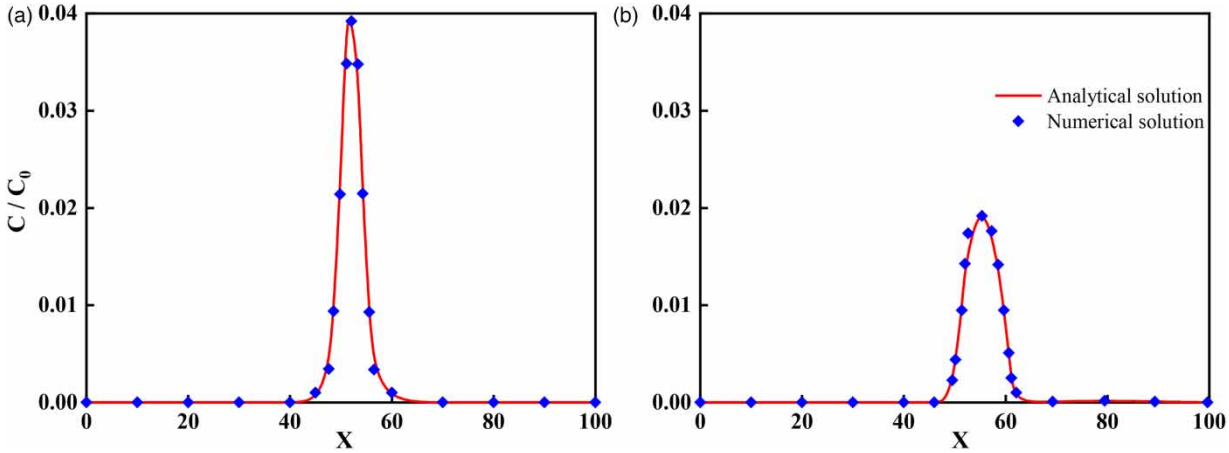

Figure 5 | Comparison of our model results with the analytical solution from Aral & Liao (1996). (a) and (b) are the dimensionless solute concentration profiles along the horizontal line $y = 50$ at time 100 and 200, respectively.

flow physics near solid surfaces and excels in capturing separated flows in intricate geometric configurations (Menter 1994). However, it is worth noting that there is still a considerable discrepancy between the mean velocity profiles obtained from our model in the vicinity of the SWI and the velocities observed in the experiments. This discrepancy can be attributed to the limited length of the porous layer in the experimental flume, which is insufficient to fully develop turbulence.

To emphasise the accuracy of the non-reactive solute model in accurately assessing the solute transport process, a test case was carried out and the results are shown in Figure 5. Point source solute is placed and released at the position (50, 50), and a flow field velocity of magnitude of 0.01 m/s is applied in the direction from left to right; the dimensionless solute concentration profiles along the horizontal line $y = 50$ at time 100 and time 200 are presented. The point source is released at the centre of the simulation region, and over time the solute gradually moves to the right with the flow field due to convective diffusion and spreads throughout the fluid domain. Comparison of the results with the analytical solution gives good agreement, indicating the reasonable validity of the non-reactive solute transport model.

3.2. Analysis of hydrodynamic results

3.2.1. Flow field characteristics

We applied the parameters listed in Table 2 to investigate the effect of $\mathrm{Re}_f = U_f H_f / \upsilon$ and the porous structures on the coupled overlying water and porous media systems. Figure 6(a) shows the mean surface velocity profile for each study case. In the

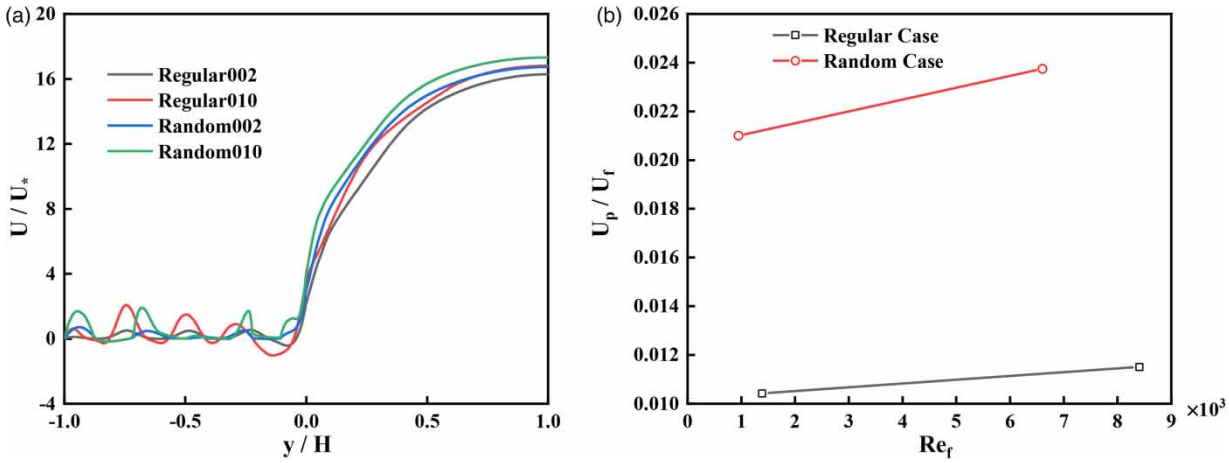

Figure 6 | (a) Mean velocity profiles of the study cases. (b) Ratios of mean porous velocity to mean surface velocity.

porous domain ($y/H < 0$), Regular010 and Random010 show that wavy pattern in the velocity profiles, in contrast to Regular002 and Random002, which show almost no change in velocity profiles, is due to the fact that the overlying water with high Re_f accelerates the exchange process between the overlying water and the pore water, which makes more water enter into the porous media layer from the overlying water layer; a larger-scale recirculation zone is formed in the pore space of the porous media layer, and the velocity distribution in the recirculation zone exhibits a wave-like pattern. For the regular porous structures (Regular002 and Regular010), the velocities are negative and less variable near the SWI, due to the fact that in the vicinity of the SWI, a large number of recirculation zones are formed at the interface due to the induction of the overlying water, which affects the exchange process between the overlying water and the porous medium, a phenomenon identical to that observed by Wang *et al.* (2021). For random porous structures (Random002 and Random010), the velocities consistently maintain positive values around the SWI, which can be attributed to the random porous structure inducing more preferential flow from the overlying water into the porous medium at the interface, and the presence of preferential flow disrupting the formation of recirculation zones, as will be discussed in Section 3.2.3.

At the same porosity, Figure 6(b) shows that the porous structures determine the U_p/U_f, where U_p is the mean velocity of the porous domain. The random porous structure will create strong preferential flow path and disrupt the formation of recirculation zones, allowing more water to enter the porous media layer from the overlying water layer, which directly affects the velocity of pore water in the porous media, and the U_p/U_f is twice as high as regular porous structures. In other words, U_p/U_f exhibits a greater sensitivity towards the pore structure as compared to Re_f, and this disparity arises from the fact that the mean velocity structure in the finite water depth is more dependent on the porous structures (Wu & Mirbod 2018; Guo *et al.* 2020).

3.2.2. Reynolds stresses

Analysis of Reynolds stresses are important for understanding and predicting the behaviour of fluid flow and the dispersion of solutes (Coceal *et al.*2007; Fang *et al.* 2018; Voermans *et al.* 2018). As shown in Figure 7, comparison of the main components of Reynolds stresses, all Reynolds stress components and Re_f are positively correlated due to greater transient velocities and larger velocity components in the transverse and longitudinal directions for high Re_f cases. For the regular porous structures, the streamwise Reynolds normal stresses τ_{xx} and shear stresses τ_{xy} peak near the SWI, while the vertical Reynolds normal stresses peak at $y/H = -0.1$ due to the intense vertical momentum exchange at the SWI. This phenomenon can be attributed to the spatial anisotropy of the flow field at the SWI and the recirculation zone close to the interface, which leads to change in the peak values of the Reynolds stress components (Mignot *et al.* 2009; Fang *et al.* 2018).

To quantify the relationship between the local slope angle and the Reynolds stresses in random porous structures, we define the angle between the first layer and the horizontal line as θ (illustrated in Figure 3(b)). The upstream slopes correspond to $\theta > 0$, while the leeward slopes correspond to $\theta < 0$. In contrast to regular porous structures, where multiple Reynolds normal

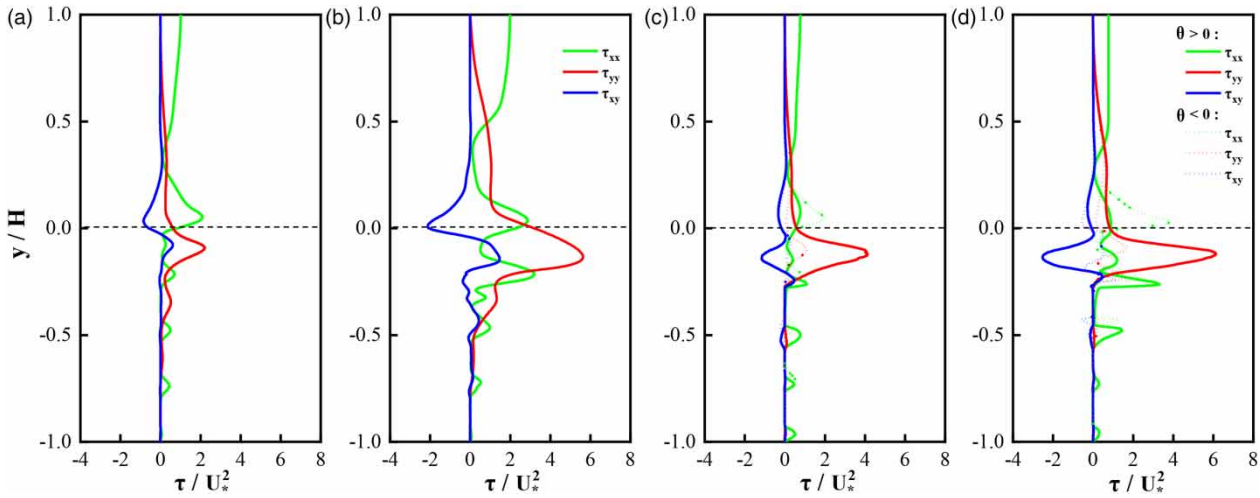

Figure 7 | Vertical profiles of Reynolds stresses components. (a)–(d) denote cases Regular002, Regular010, Random002, and Random010, respectively.

stress components peak at the SWI, random porous structures exhibit a unique behaviour wherein only the streamwise Reynolds normal stresses τ_{xx} peak at the SWI. This is due to the fact that the arrangement of the random porous structures favours the generation of a more stable preferential flow, allowing more overlying water to participate in the water exchange process, which in turn disrupts the formation of the recirculation zone in the porous media layer.

The peak of vertical Reynolds normal stresses τ_{yy} and shear stresses τ_{xy} exhibit significantly higher values on the upstream slopes compared to the leeward slopes; this is due to the formation of preferential flow, which leads to enhanced vertical exchange of overlying water across the SWI into the porous media layer occurring, and the transient vertical flow velocity is larger. However, the streamwise Reynolds normal stresses τ_{xx} on the leeward slopes are higher than those on the upstream slope due to the presence of recirculation zones on the leeward slope, which slows down the streamwise instantaneous velocity in the overlying water; thus, the leeward and upstream slope show differences.

3.2.3. Flow paths and recirculation zones

The momentum exchange between the overlying water layer and the porous layer is related to the turbulence intensity and slip velocity at the interface, leading to a recirculation zone near the SWI (Breugem & Boersma 2005; Kim *et al.* 2020; Shen *et al.* 2021). To evaluate the influence of regular and random porous structures on flow paths and recirculation zones, we selected Regular010 and Random010 as representative examples (illustrated in Figure 8). It can be seen that the flow paths of Regular010 and Random010 within the porous media layer are completely different, which is due to the fact that the preferential flow paths depend largely on the arrangement of the porous structure. The random porous structures induce more preferential flow paths, which promote the water to enter the porous media layer from the overlying water layer and accelerate the water exchange process. Therefore, the preferential flow pattern should not be neglected in considering the exchange process between the overlying water and the porous media layer.

As a consequence of the swift reduction in turbulence within the overlying water towards the porous layer, solute exchange is predominantly affected in the vicinity of the interface (Figure 4). The recirculation zones and turbulence characteristics near the SWI are considered to be the key factors controlling the mass transfer between the overlying water and the porous layer (Tonina & Buffington 2007; Roche *et al.* 2018). As shown in Figure 8, the size and location of the recirculation zone strongly depend on the arrangement of the porous structures. More recirculation zones exist in the regular porous structures than in the random porous structures, which are mainly due to the interfacial momentum exchange inherent in the porous space, and the random porous structures will induce a more preferential flow, thus limiting the formation of recirculation zones in the porous media layer. For random porous structures, recirculation zones are mainly found on leeward slopes due to the significantly lower Reynolds stresses compared to upstream slopes and the relatively low flow velocities on leeward slopes, which are favourable for the formation of recirculation zones. Furthermore, in the random porous structures, the existence of preferential flow inhibits the formation of the recirculation zone in the porous media layer, which accelerates the escape of solutes from the recirculation zone, and to some extent reduces the residence time of solutes in the porous layer. The connection between the recirculation zones and solute transport is discussed further in Section 3.3.

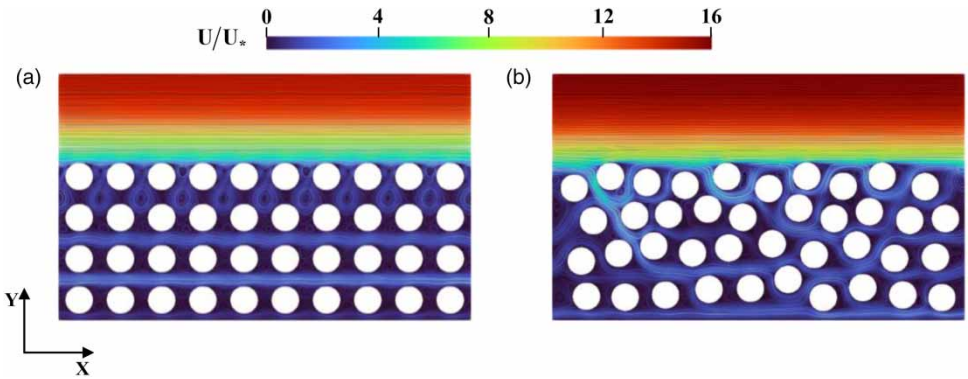

Figure 8 | Mean flow velocity distribution and flow paths for (a) Regular010 and (b) Random010.

3.3. Analysis of point source dispersion

3.3.1. Spatial concentration distribution

After turbulence is sufficiently developed, we set up a continuously releasing point source at $y/H = 0$. The characteristics of the spatial distribution of solutes in the coupled model are basically unchanged after 500 s of release from the point source; thus, we chose the time-averaged results after 500 s of release as the study moment, as shown in Figure 9. The closer to the point source release location, the higher the concentration of the surrounding solute (Guo *et al.* 2022). With the increase of Re_f, the influence range of point source pollution gradually reduces, which is due to the enhancement of convection in the overlying water, which promotes the solute exchange process between the overlying water layer and the porous media layer and accelerates the diffusion of solutes in the water body. Based on the comparison in Figure 9, under identical hydrodynamic conditions, it is evident that the concentration of solutes within the random porous structures is higher and demonstrates a broader range of influence. This is due to the fact that the random porous structures will induce more preferential flow paths relative to the regular porous structures, and strong exchange interactions will occur at the SWI, accelerating the entry of solutes from the overlying water into the porous media layer, so that the solutes will reach deeper into the porous media rather than being confined to the interface.

To further quantify the extent of the impact of point source releases, we extracted the vertical distribution of solute concentrations at $x = 0.03$, 0.06, 0.09, and 0.12 m, respectively (Figure 10). The peak solute concentration decreases with distance from the release location of the point source, which is due to the fact that the solute transport process is a combination of convective action in the water column and vertical turbulent diffusivity, which is also consistent with previous work (Ai *et al.* 2022). As shown in Figure 10(a) and 10(b), for regular porous structures, the peak solute concentration near the SWI, which is approximately normally distributed, is due to the strong exchange interaction between the overlying water and the pore water at the SWI, which generates a large number of vortices and creates a recirculation zone in the pore space and serves as a transient retention zone for the solutes, resulting in a peak solute concentration degree at the interface. In the case of random porous structures (Figure 10(c) and 10(d)), the solute concentration distribution exhibits significant irregularity, which is attributed to the presence of preferential flow prevent the formation of recirculation zones. The peak concentration is predominantly concentrated below the SWI, which is approximately four times higher than that observed in regular porous structures.

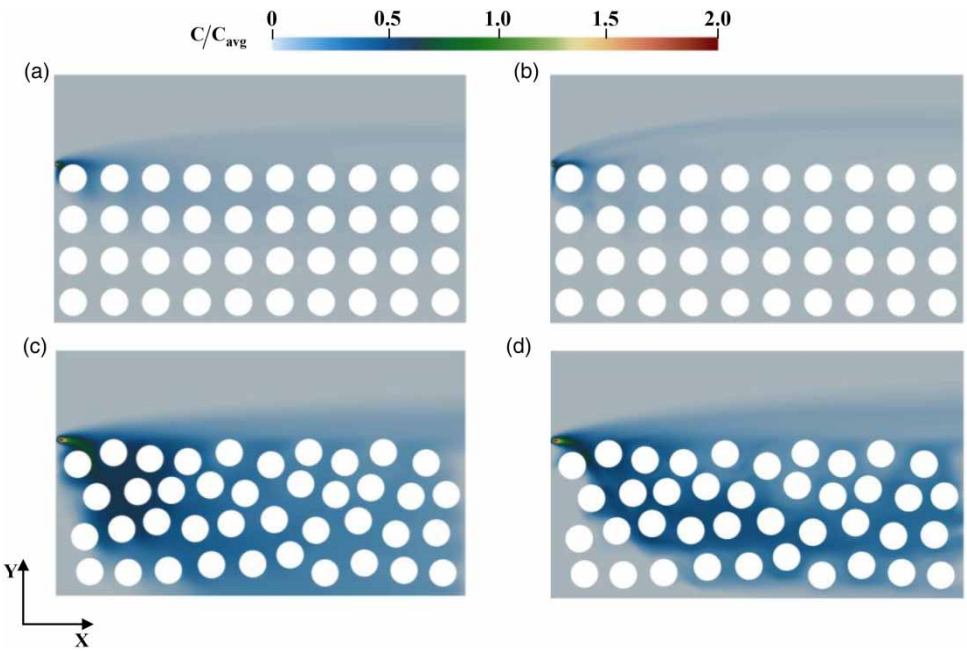

Figure 9 | Spatial concentration distribution. (a)–(d) denote cases Regular002, Regular010, Random002, and Random010, respectively.

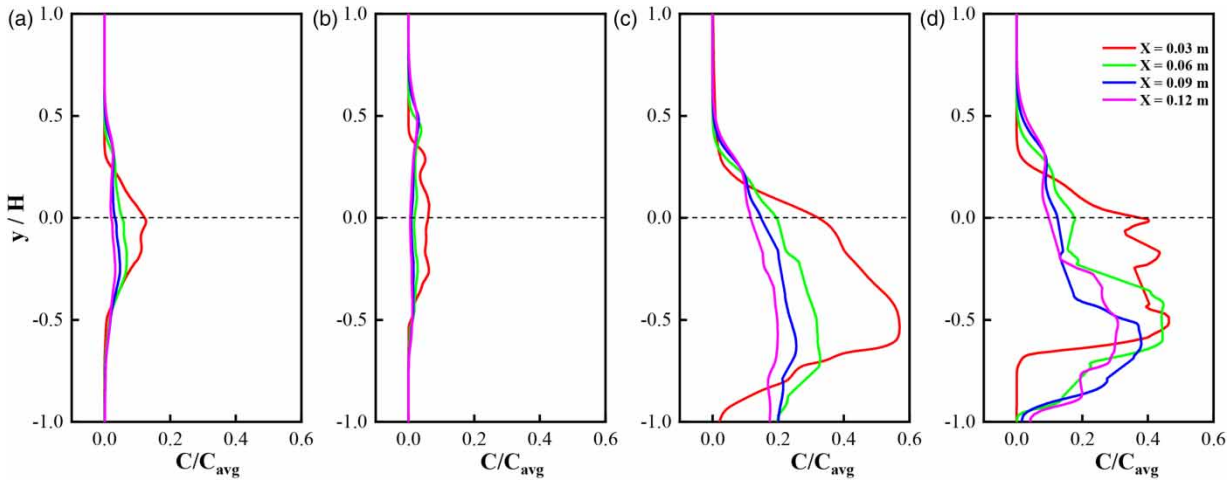

Figure 10 | Vertical distribution of solute concentrations at different locations. (a)–(d) denote cases Regular002, Regular010, Random002, and Random010, respectively.

3.3.2. Turbulent solute flux

Here, we utilised the turbulent solute flux to quantify the characteristics of the turbulent transport of solute, which can be calculated by the following equation:

$$\overline{u_i' c'} = \overline{u_i c} - \overline{u_i}\,\overline{c} \tag{10}$$

where represents the time-averaged value of the variable; u_i and c are the velocity vector and the solute concentration, respectively, which can be defined as follows:

$$\overline{u_i} = u_i - u_i' \tag{11}$$

$$\bar{c} = c - c' \tag{12}$$

where u_i' and c' are the fluctuating values for velocity and solute, respectively.

Figure 11 shows the distribution of turbulent solute flux. As can be seen, the turbulent solute flux increases with Re_f, with the highest concentration distribution observed near the point source, and the peak is predominantly located at the interface and the region above it. This is due to the interaction of turbulence with the porous structures, which is strongest at the SWI and forms a large number of vortex structures above the SWI, enhancing solute mixing in this region. Random porous structures have stronger turbulent solute fluxes compared to regular porous structures, which further explains the wider distribution of solute concentrations in random porous structures.

Concretely, the vertical profiles of the transverse turbulent solute flux $\overline{u'c'}$ and the longitudinal turbulent solute flux $\overline{v'c'}$ are shown in Figure 12. The transverse turbulent solute flux $\overline{u'c'}$ is significantly higher than the longitudinal turbulent solute flux $\overline{v'c'}$, which is due to the fact that the instantaneous velocity in the transverse direction is obviously higher than that in the longitudinal direction, which leads to a more obvious phenomenon of solute transport in the streamwise direction. The peak of the transverse turbulent solute flux $\overline{u'c'}$ remains consistent regardless of the profile location, which is attributed to the turbulent advection that dominates the solute transport process in the transverse direction, significantly more than the diffusion of the solute in the transverse direction, and therefore the position of the peak does not change. In contrast, the peak of the longitudinal turbulent solute flux $\overline{v'c'}$ is related to the location of the release from the point source, with larger values observed at closer distance, which is due to the fact that the vertical component of the instantaneous velocity is smaller and the diffusion of solutes in the vertical direction dominates the transport process.

The presence of an inverse distribution of turbulent solute fluxes in the porous media layer is due to the shear interaction between the porous structures. For regular porous structures, the peak of the turbulent solute flux is located above the SWI,

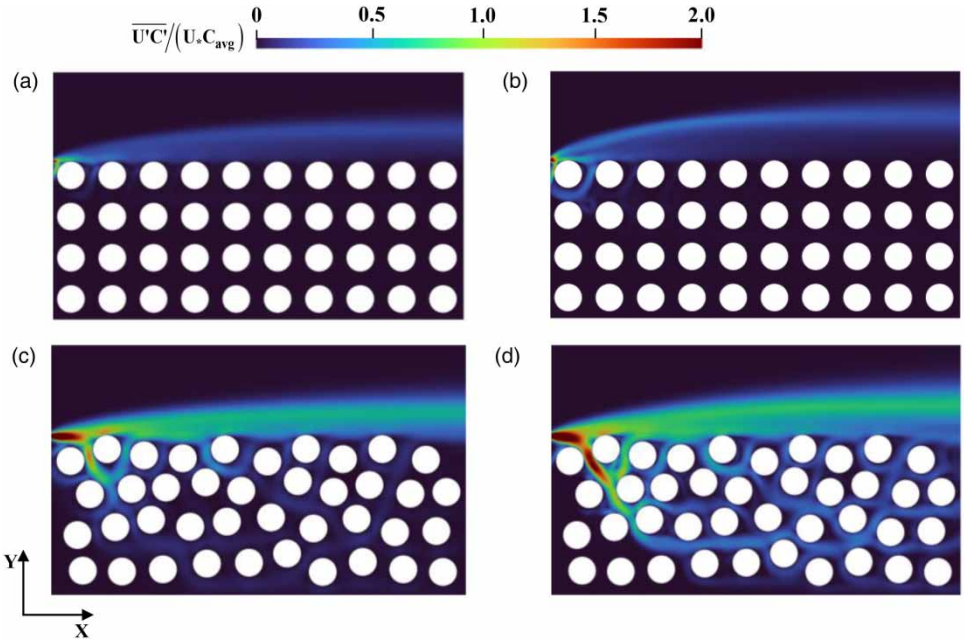

Figure 11 | Distribution of the turbulent solute flux relative to the mean flux, which indicates the characteristics of the turbulent transport of solute. (a)–(d) denote cases Regular002, Regular010, Random002, and Random010, respectively.

whereas the peak for random porous structures is closer to the SWI and highly irregular. This is due to the presence of preferential flow in the random porous structures, which weakens the turbulence intensity above the interface, and more water enter the porous media layer, which explains why the solute distribution in the random porous structures is more widespread.

3.3.3. Effects of point release position

In fact, under identical flow conditions, the position of the point source release can greatly influence the distribution of solute concentrations, which is of great significance for environmental applications such as wastewater treatment (Li 2014; Hou *et al.* 2021). As we delve into the impact of the point source release position in this section, for the sake of brevity, we adopt case002 (Regular002 and Random002) as the reference for point source release at $y/H = 0.5$ and 1, respectively.

As shown in Figure 13, the peak vertical concentration of solutes is always close to the release height due to the different release locations of the point sources and decreases with increasing distance from the release source. This is due to the fact that at the moment of solute release from the point source, with the turbulent interaction of the overlying water, the velocity component along the flow direction is larger and dominates the solute transport process. Compared to the height of release at $y/H = 0.5$, the peak solute concentration is higher when the point source releases at $y/H = 0.5$, which indicates that the rate of solute mixing will accelerate as the point source release position is closer to the riverbed. Compared with the regular pore structure, the vertical concentration peak of the random porous structure is slightly higher, which is due to its larger vertical turbulent diffusion coefficient and velocity gradient. Therefore, the release position of the point source also significantly affects the distribution characteristics of solutes in the porous media layer. The above analyses can be applied to numerous environmental and engineering projects, such as the selection of discharge points for industrial wastewater.

4. CONCLUSION

In this study, we focus on investigating the significance of randomly distributed porous structures within coupled overlying water and porous media, employing pore-scale numerical simulations. The primary objective is to explore the turbulent characteristics and point source solute transport across the SWI. This research question holds significant implications for the study of fluid flow and transport in coupled systems of surface flow and porous media, spanning various research areas, including procedural water treatment (Wilhelm. 2009; Hou *et al.* 2021), riverbeds (Blois *et al.* 2014; Hester *et al.* 2019), continental shelf sediments (Huettel *et al.* 2014), porous media (Yang *et al.* 2014; Wang *et al.* 2023), and marine particles (Ahmerkamp *et al.* 2022). In particular, the application in the field of water treatment, which covers the selection of

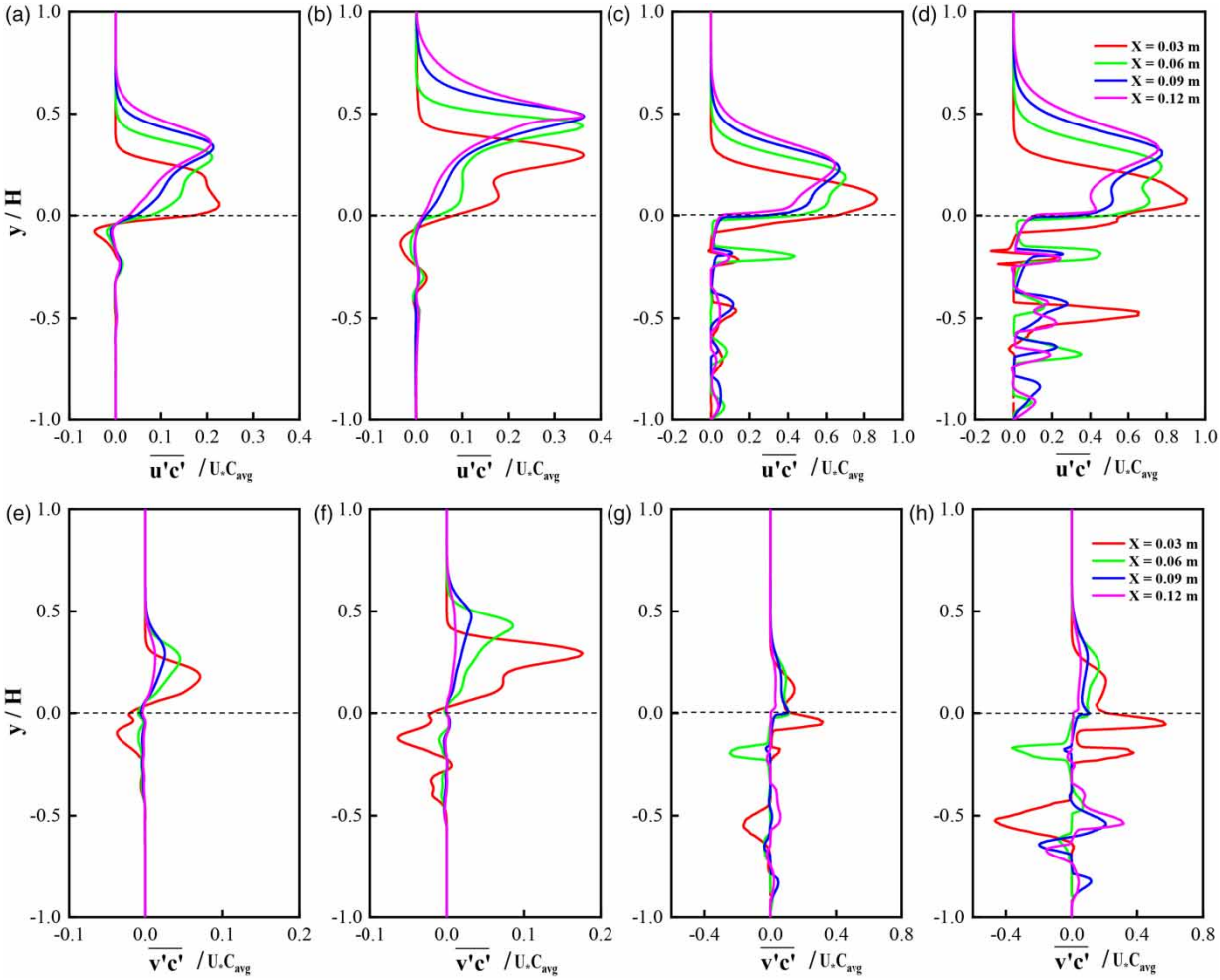

Figure 12 | Vertical profiles of the transverse turbulent solute flux $\overline{u'c'}$ and the longitudinal turbulent solute flux $\overline{v'c'}$. (a) and (e) Regular002; (b) and (f) Regular010; (c) and (g) Random002; (d) and (h) Random010.

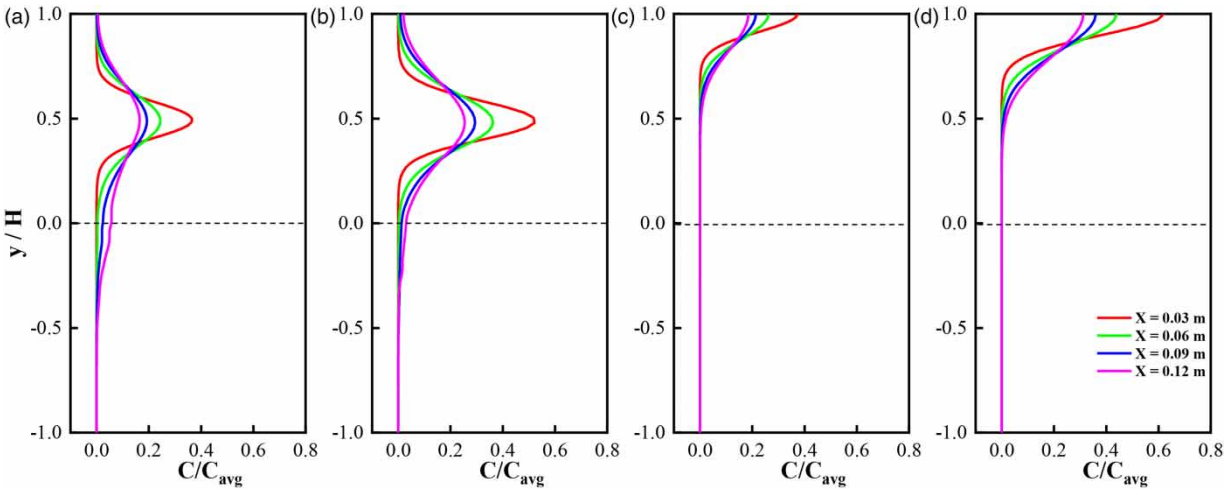

Figure 13 | Vertical concentration distribution of point source release at $y/H = 0.5$ of (a) Regular002 and (b) Random002; and point source release at $y/H = 1$ of (c) Regular002 and (d) Random002.

industrial wastewater discharge points and urban domestic sewage discharge points, is of guiding significance for river pollution management.

The hydrodynamic properties of both the overlying water and the porous domain are highly sensitive to the configuration of porous structures. Compared with regular porous structures, random porous structures induce a more preferential flow, prompting a greater influx of overlying water into the porous media layer through the SWI, consequently accelerating the solute transport process. As the Reynolds number Re_f increases, the Reynolds stresses exhibit a positive correlation with the flow velocity in the porous domain, resulting in stronger variabilities of the velocity distribution. The peak Reynolds stresses are higher in the case of random porous structures compared to regular ones, favouring a more stable preferential flow pattern and reducing the extent of recirculation zones. The alteration of porous structures significantly influences the flow paths and the formation of recirculation zones. The presence of preferential flow inhibits the formation of recirculation zones, accelerates the escape of solutes from these zones, and reduces the residence time of solutes in the porous layer.

The proximity to the point source release directly affects the solute concentration in the surrounding water column, and convection in the overlying water accelerates the diffusion of solutes. When compared under the same conditions, the random porous structures exhibit higher solute concentrations and have a broader influence compared to regular porous structures. This behaviour can be attributed to preferential flow, which allows solutes to penetrate deeper into the porous layer, peaking at four times the value observed in regular porous structures. The wider distribution of solutes in random porous structures is explained by the turbulent solute flux, where the presence of a shear layer leads to an inverse distribution of longitudinal turbulent solute flux. Furthermore, the position of the point source release substantially influences the distribution of solute concentration, consistently resulting in the peak concentration coinciding with the height of the point source release. Moreover, as the release point approaches the riverbeds, the mixing of solutes accelerate at a faster rate.

In conclusion, this study serves as a logical first step in elucidating the influence of porous structures on flow and point source dispersion within a coupled system of overlying water and porous media. Although this study is based on a mathematical model analysing in detail the flow and point source transport mechanisms in a coupled system of overlying water and porous media, complementary experiments using particle image velocimetry (PIV) and laser-induced fluorescence will further enhance our understanding of such issues. Moving forward, further research and improvements are required in the following areas: (1) conducting experimental studies complementary to numerical modelling; (2) more comprehensive investigation into the link between preferential flow trajectories and the arrangement of pore structures; (3) expansion of the model into a 3D representation to explore spanwise flow and point source dispersion in greater detail; and (4) integration of reactive solutes to better understand the impact on biogeochemical transformation. Addressing these aspects will provide valuable insights and contribute to a deeper understanding of the interactions between porous structures, flow dynamics, and solute dispersion.

ACKNOWLEDGEMENTS

This study was supported by the National Key R&D Program of China (2022YFC3202600), the National Natural Science Foundation of China (52309086), and the Water Conservancy Science and Technology Project in Jiangsu Province (2023013, 2022061). S. A. acknowledges funding by Novo Nordisk Fonden (MATIC) and the Max Planck Society. G. B. was funded through the Cluster of Excellence 'The Ocean Floor-Earth's Uncharted Interface', MARUM of the Universität Bremen, Germany.

DATA AVAILABILITY STATEMENT

All relevant data are included in the paper or its Supplementary Information.

CONFLICT OF INTEREST

The authors declare there is no conflict.

REFERENCES

Ahmerkamp, S., Winter, C., Janssen, F., Kuypers, M. M. & Holtappels, M. 2015 The impact of bedform migration on benthic oxygen fluxes. *Journal of Geophysical Research: Biogeosciences* **120**, 2229–2242. https://doi.org/10.1002/2015JG003106.

Ahmerkamp, S., Liu, B., Kindler, K., Maerz, J., Stocker, R., Kuypers, M. & Khalili, A. 2022 Settling of highly porous and impermeable particles in linear stratification: Implications for marine aggregates. *Journal of Fluid Mechanics* **931**, A9. https://doi.org/10.1017/jfm.2021.913.

Ai, Y., Dai, H., Zhai, Y., Chen, B. & Huai, W. 2022 The effect of solute release position on transient solute dispersion in floating wetlands: An analytical study. *Journal of Cleaner Production* **369**, 133370. https://doi.org/10.1016/j.jclepro.2022.133370.

Aral, M. M. & Liao, B. 1996 Analytical solutions for two-dimensional transport equation with time-dependent dispersion coefficients. *Journal of Hydrologic Engineering* **1** (1), 20. https://doi.org/10.1061/(ASCE)1084-0699(1996)1:1(20).

Bartzke, G., Podszun, L. & Huhn, K. 2014 On the role of fluid infiltration into gravel dunes – Using a 3D numerical model. *Marine Geology* **380**, 231–244. https://doi.org/10.1016/j.csr.2016.02.006.

Blois, G., Smith, G. S., Best, J. L., Hardy, R. J. & Lead, J. R. 2012 Quantifying the dynamics of flow within a permeable bed using time-resolved endoscopic particle imaging velocimetry (EPIV). *Experiments in Fluids* **53** (1), 51–76. https://doi.org/10.1007/ s00348-011-1198-8.

Blois, G., Best, J. L., Sambrook Smith, G. H. & Hardy, R. J. 2014 Effect of bed permeability and hyporheic flow on turbulent flow over bed forms. *Geophysical Research Letter* **41**. https://doi.org/10.1002/2014GL060906.

Boano, F., Harvey, J. W., Marion, A., Packman, A. I., Revelli, R., Ridolfi, L. & Wörman, A. 2014 Hyporheic flow and transport processes: Mechanisms, models, and biogeochemical implications. *Reviews of Geophysics* **52** (4), 603–679. https://doi.org/10.1002/2012RG000417.

Bolster, D., Méheust, Y., Le Borgne, T., Bouquain, J. & Davy, P. 2014 Modeling preasymptotic transport in flows with significant inertial and trapping effects – The importance of velocity correlations and a spatial Markov model. *Advances in Water Resources* **70**, 89–103. https://doi.org/10.1016/j.advwatres.2014.04.014.

Bottero, S., Storck, T., Heimovaara, T. J., van Loosdrecht, M. C., Enzien, M. V. & Picioreanu, C. 2013 Biofilm development and the dynamics of preferential flow paths in porous media. *Biofouling* **29** (9), 1069–1086. https://doi.org/10.1080/08927014.2013.828284.

Breugem, W. P. & Boersma, B. J. 2005 Direct numerical simulations of turbulent flow over a permeable wall using a direct and a continuum approach. *Physics of Fluids* **17** (2), 025103. https://doi.org/10.1063/1.1835771.

Cardenas, M. B. & Wilson, J. L. 2007a Hydrodynamics of coupled flow above and below a sediment-water interface with triangular bed forms: Underflow case. *Advances in Water Resources* **30**, 301–313. https://doi.org/10.1016/j.advwatres.2006.06.009.

Chen, X., Cardenas, M. B. & Chen, L. 2018 Hyporheic exchange driven by three-dimensional sandy bed forms: Sensitivity to and prediction from bed form geometry. *Water Resources Research* **54**, 4131–4149. https://doi.org/10.1029/2018WR022663.

Cho, J. Y., Lee, H. M., Kim, J. H., Lee, W. & Lee, J. S. 2022 Numerical simulation of gas-liquid transport in porous media using 3D color-gradient lattice Boltzmann method: Trapped air and oxygen diffusion coefficient analysis. *Engineering Applications of Computational Fluid Mechanics* **16** (1), 177–195. https://doi.org/10.1080/19942060.2021.2008012.

Coceal, O., Dobre, A., Thomas, T. G. & Belcher, S. E. 2007 Structure of turbulent flow over regular arrays of cubical roughness. *Journal of Fluid Mechanics* **589**, 375–409. https://doi.org/10.1017/S002211200700794X.

Crevacore, E., Tosco, T., Sethi, R., Boccardo, G. & Marchisio, D. L. 2016 Recirculation zones induce non-Fickian transport in three-dimensional periodic porous media. *Physical Review E* **94** (5), 053118. https://doi.org/10.1103/PhysRevE.94.053118.

Fang, H. W., Han, X., He, G. J. & Dey, S. 2018 Influence of permeable beds on hydraulically macro-rough flow. *Journal of Fluid Mechanics* **847**, 552–590. https://doi.org/10.1017/jfm.2018.314.

Grant, S. B., Stewardson, M. J. & Marusic, I. 2012 Effective diffusivity and mass flux across the sediment-water interface in streams. *Water Resources Research* **48**, W05548. https://doi.org/10.1029/2011WR011148.

Guo, J. & Chen, G. 2022 Solute dispersion from a continuous release source in a vegetated flow: An analytical study. *Water Resources Research* **58** (4). https://doi.org/10.1029/2021wr030255.

Guo, C., Li, Y., Nian, X., Xu, M. & Wang, Y. 2020 Experimental study on the slip velocity of turbulent flow over and within porous media. *Physics of Fluids* **32** (1), 015111. https://doi.org/10.1063/1.5128479.

Han, X., Fang, H. W., He, G. J. & Reible, D. 2018 Effects of roughness and permeability on solute transfer at the sediment water interface. *Water Research* **129**, 39–50. https://doi.org/10.1016/j.watres.2017.10.049.

He, G. J., Han, X., Fang, H. W., Reible, D. & Huang, L. 2019 Effects of roughness Reynolds number on scalar transfer mechanisms at the sediment-water interface. *Water Resources Research* **55**. https://doi.org/10.1029/2018WR024493.

Hester, E. T., Young, K. I. & Widdowson, M. A. 2013 Mixing of surface and groundwater induced by riverbed dunes: Implications for hyporheic zone definitions and pollutant reactions. *Water Resources Research* **49** (9), 5221–5237. https://doi.org/10.1002/wrcr.20399.

Hester, E. T., Eastes, L. A. & Widdowson, M. A. 2019 Effect of surface water stage fluctuation on mixing-dependent hyporheic denitrification in riverbed dunes. *Water Resources Research* **55** (6), 4668–4687. https://doi.org/10.1029/2018WR024198.

Hou, X., Qin, L., Xue, X., Xu, S., Yang, Y., Liu, X. & Li, M. 2021 A city-scale fully controlled system for stormwater management: Consideration of flooding, non-point source pollution and sewer overflow pollution. *Journal of Hydrology* **603**. https://doi.org/10.1016/j.jhydrol.2021.127155.

Huettel, M., Berg, P. & Kostka, J. E. 2014 Benthic exchange and biogeochemical cycling in permeable sediments. *Annual Review of Marine Science* 23–51. https://doi.org/10.1146/annurev-marine-051413-012706.

Janssen, F., Cardenas, M. B., Sawyer, A. H., Dammrich, T., Krietsch, J. & de Beer, D. 2012 A comparative experimental and multiphysics computational fluid dynamics study of coupled surface–subsurface flow in bed forms. *Water Resources Research* **48**. https://doi.org/10.1029/2012WR011982.

Jin, G. Q., Tang, H. W., Gibbes, B., Li, L. & Barry, D. A. 2010 Transport of nonsorbing solutes in a streambed with periodic bedforms. *Advances in Water Resources* **33** (11), 1402–1416. https://doi.org/10.1016/j.advwatres.2010.09.003.

Kim, J. S. & Kang, P. K. 2020 Anomalous transport through free-flow-porous media interface: Pore-scale simulation and predictive modeling. *Advances in Water Resources* **135** (103467), 1–12. https://doi.org/10.1016/j.advwatres.2019.103467.

Kim, J. S., Kang, P. K., He, S., Shen, L., Kumar, S. S., Hong, J. & Seo, W. 2023 Pore-scale flow effects on solute transport in turbulent channel flows over porous media. *Transport in Porous Media* **146**, 223–248. https://doi.org/10.1007/s11242-021-01736-6.

Lee, A., Aubeneau, A., Liu, X. & Cardenas, M. B. 2021 Hyporheic exchange in sand dunes under a freely deforming river water surface. *Water Resources Research* **57**, e2020WR028817. https://doi.org/10.1029/2020WR028817.

Li, W. C. 2014 Occurrence, sources, and fate of pharmaceuticals in aquatic environment and soil. *Environmental Pollution* **187**, 193–201. https://doi.org/10.1016/j.env pol.2014.01.015.

Lian, Y. P., Dallmann, J., Sonin, B., Roche, K. R., Liu, W. K., Packman, A. I. & Wagner, G. J. 2019 Large eddy simulation of turbulent flow over and through a rough permeable bed. *Computers & Fluids* **180**, 128–138. https://doi.org/10.1016/j.compfluid.2018.12.015.

Menter, F. R. 1993 Zonal two equation k-ω turbulence models for aerodynamic flows. In *23rd Fluid Dynamics, Plasmadynamics, and Lasers Conference*, p. 2906. https://doi.org/10.2514/6.1993-2906.

Menter, F. R. 1994 Two-equation eddy-viscosity turbulence models for engineering applications. *AIAA Journal* **32** (8), 1598–1605. https://doi.org/10.2514/3.12149.

Menter, F. R., Kuntz, M. & Langtry, R. 2003 Ten years of industrial experience with the SST turbulence model. *Heat and Mass Transfer* **4** (1), 625–632.

Mignot, E., Barthelemy, E. & Hurther, D. 2009 Double-averaging analysis and local flow characterization of near-bed turbulence in gravel-bed channel flows. *Journal of Fluid Mechanics* **618**, 279–303. https://doi.org/10.1017/S0022112008004643.

Pal, A., Gin, K. Y., Lin, A. Y. & Reinhard, M. 2010 Impacts of emerging organic contaminants on freshwater resources: Review of recent occurrences, sources, fate and effects. *Science of The Total Environment* **408** (2010), 6062–6069. https://doi.org/10.1016/j.scito tenv. 2010.09.026.

Prinos, P., Sofialidis, D. & Keramaris, E. 2003 Turbulent flow over and within a porous bed. *Journal of Hydraulic Engineering* **129** (9), 720–733. https://doi.org/10.1061/(ASCE)0733-9429(2003)129:9(720).

Reidenbach, M. A., Limm, M., Hondzo, M. & Stacey, M. T. 2010 Effects of bed roughness on boundary layer mixing and mass flux across the sediment-water interface. *Water Resources Research* **46**, W07530. https://doi.org/10.1029/2009WR008248.

Roche, K. R., Blois, G., Best, J. L., Christensen, K. T., Aubeneau, A. F. & Packman, A. I. 2018 Turbulence links momentum and solute exchange incoarse-grained streambeds. *Water Resources Research* **54**. https://doi.org/10.1029/2017WR021992.

Rubol, S., Battiato, I. & de Barros, F. P. J. 2016 Vertical dispersion in vegetated shear flows. *Water Resources Research* **52** (10), 8066–8080. https://doi.org/10.1002/2016wr018907.

Sarmiento-Laurel, C., Cardemil, J. M. & Calderón-Muñoz, W. R. 2022 Local entropy generation model for numerical CFD analysis of fluid flows through porous media, under laminar and turbulent regimes. *Engineering Applications of Computational Fluid Mechanics* **16** (1), 804–825. https://doi.org/10.1080/19942060.2022.2040595.

Scalo, C., Piomelli, U. & Boegman, L. 2012 Large-eddy simulation of oxygen transfer to organic sediment beds. *Journal of Geophysical Research Atmospheres* **117**, C06005. https://doi.org/10.1029/2011JC007289.

Shen, G., Yuan, J. & Phanikumar, M. S. 2020 Direct numerical simulations of turbulence and hyporheic mixing near sediment–water interfaces. *Journal of Fluid Mechanics* **892**, A20. https://doi.org/10.1017/jfm.2020.173.

Shen, G., Yuan, J. & Phanikumar, M. S. 2021 Quantifying the effects of bed roughness on transit time distributions via direct numerical simulations of turbulent hyporheic exchange. *Water Resources Research* **58**, e2021WR030503. https://doi.org/10.1029/2021WR030503.

Singh, V. K., Panda, K. C., Sagar, A., Al-Ansari, N., Duan, H. F., Paramaguru, P. K., Vishwakarma, D. K., Kumar, A., Kumar, D., Kashyap, P. S., Singh, R. M. & Elbeltagi, A. 2022 Novel genetic algorithm (GA) based hybrid machine learning-pedotransfer function (ML-PTF) for prediction of spatial pattern of saturated hydraulic conductivity. *Engineering Applications of Computational Fluid Mechanics* **16** (1), 1082–1099. https://doi.org/10.1080/19942060.2022.2071994.

Suga, K., Okazaki, Y. & Kuwata, Y. 2020 Characteristics of turbulent square duct flows over porous media. *Journal of Fluid Mechanics* **884**, A7. https://doi.org/10.1017/jfm.2019.914.

Tanino, Y. & Nepf, H. M. 2008 Lateral dispersion in random cylinder arrays at high Reynolds number. *Journal of Fluid Mechanics* **600**, 339–371. https://doi.org/10.1017/s0022112008000505.

Tonina, D. & Buffington, J. M. 2007 Hyporheic exchange in gravel bed rivers with pool-riffle morphology: Laboratory experiments and three-dimensional modeling. *Water Resources Research* **43**, W01421. https://doi.org/10.1029/2005WR004328.

Van Balen, W., Uijttewaal, W. S. J. & Blanckaert, K. 2010 Large-eddy simulation of a curved open-channel flow over topography. *Physics of Fluids* **22** (7), 075108. https://doi.org/10.1063/1.3459152.

Voermans, J. J., Ghisalberti, M. & Ivey, G. N. 2017 The variation of flow and turbulence across the sediment-water interface. *Journal of Fluid Mechanics* **824**, 413–437. https://doi.org/10.1017/jfm.2017.345.

Voermans, J. J., Ghisalberti, M. & Ivey, G. N. 2018 The hydrodynamic response of the sediment-water interface to coherent turbulent motions. *Geophysical Research Letter* **45**, 10520–10527. https://doi.org/10.1029/2018GL079850.

Wang, W. K., Yang, G., Evrim, C., Terzis, A., Helmig, R. & Chu, X. 2021 An assessment of turbulence transportation near regular and random permeable interfaces. *Physics of Fluids* **33** (11), 115103. https://doi.org/10.1063/5.0069311.

Wang, X., Qi, W., Li, Y., Wu, L. & Wang, Y. 2023 Study on the clogging pattern of multi-graded microparticles in porous asphalt concrete. *AQUA Water Infrastructure, Ecosystems and Society* jws2023124. https://doi.org/10.2166/aqua.2023.124.

Wilhelm, F. M., 2009 Pollution of aquatic ecosystems I. In: *Encyclopedia of Inland Waters* (Likens, G. E., ed.). Academic Press, Oxford, pp. 110–119. https://doi.org/10.1016/b978-012370626-3.00222-2.

Wu, Z. & Mirbod, P. 2018 Experimental analysis of the flow near the boundary of random porous media. *Physics of Fluids* **30** (4), 047103. https://doi.org/10.1063/1.5021903.

Wu, X., Jiang, Q. & Ma, T. 2023 Geochemical processes of phosphorus-iron on sediment-water interface during discharge of groundwater to freshwater lakes: Kinetic and mechanistic insights. *Science of The Total Environment* **901**, 165962. https://doi.org/10.1016/j.scitotenv.2023.165962.

Yang, Y., Zhang, T. & Zhu, D. Z. 2014 Influence of porous media on intrusion rate into water distribution pipes. *Journal of Water Supply: Research and Technology-Aqua* **63** (1), 43–50. https://doi.org/10.2166/aqua.2013.213.

Zhou, J. Q., Wang, L., Chen, Y. F. & Cardenas, M. B. 2019 Mass transfer between recirculation and main flow zones: Is physically based parameterization possible? *Water Resources Research* **55** (1), 345–362. https://doi.org/10.1029/2018WR023124.

First received 9 November 2023; accepted in revised form 3 January 2024. Available online 11 January 2024